

Have greenhouse gases intensified the contrast between wet and dry regions?

D. Polson,¹ G. C. Hegerl,¹ R. P. Allan,² and B. Balan Sarojini³

Received 12 July 2013; revised 27 August 2013; accepted 29 August 2013; published 13 September 2013.

[1] While changes in land precipitation during the last 50 years have been attributed in part to human influences, results vary by season, are affected by data uncertainty and do not account for changes over ocean. One of the more physically robust responses of the water cycle to warming is the expected amplification of existing patterns of precipitation minus evaporation. Here, precipitation changes in wet and dry regions are analyzed from satellite data for 1988–2010, covering land and ocean. We derive fingerprints for the expected change from climate model simulations that separately track changes in wet and dry regions. The simulations used are driven with anthropogenic and natural forcings combined, and greenhouse gas forcing or natural forcing only. Results of detection and attribution analysis show that the fingerprint of combined external forcing is detectable in observations and that this intensification of the water cycle is partly attributable to greenhouse gas forcing. **Citation:** Polson, D., G. C. Hegerl, R. P. Allan, and B. Balan Sarojini (2013), Have greenhouse gases intensified the contrast between wet and dry regions?, *Geophys. Res. Lett.*, 40, 4783–4787, doi:10.1002/grl.50923.

1. Introduction

[2] As temperatures rise in response to increasing greenhouse gas concentrations, the global water cycle is expected to intensify [Allen and Ingram, 2002; Trenberth et al., 2003]. This should lead to increasing atmospheric water vapor and moisture transport, from water exporting to importing regions, enhancing existing patterns of precipitation (P) minus evaporation (E) [Held and Soden, 2006; Seager and Naik, 2012]. Due to energy budget constraints in the atmosphere, the precipitation response in models is 2–3% K⁻¹ [Held and Soden, 2006; Stephens and Ellis, 2008], less than the increase in the water vapor concentrations of ~7% K⁻¹ near to the surface [Santer et al., 2007; Willett et al., 2010].

[3] The pattern of wet regions becoming wetter and dry regions becoming drier is seen in multiple satellite-based data sets of precipitation [Liu et al., 2012; Chou et al., 2013] in studies of atmospheric moisture transport using reanalysis

data [Zahn and Allan, 2011], modeling studies of past and projected changes [Sun et al., 2007; Seager and Naik, 2012; Lau et al., 2013; Liu and Allan, 2013] and changes suggested by ocean salinities [Durack et al., 2012]. It is also consistent with a wider frequency distribution of precipitation [Lintner et al., 2012; Giorgi et al., 2011; Biasutti, 2013].

[4] Changes in zonally averaged land precipitation since the 1950s have been partly attributed to anthropogenic forcing [Zhang et al., 2007; Polson et al., 2013] using fingerprint detection and attribution (D+A) methods. Changes over land and ocean combined should show higher signal-to-noise ratio [Balan Sarojini et al., 2012] and the expected change pattern is less clear over land than oceans [Held and Soden, 2006]. Here we apply a D+A analysis [Allen and Stott, 2003] to satellite data for land and ocean precipitation for the years 1988 to 2010. This is a short timescale for analyzing precipitation trends compared to natural variability; however, Seager and Naik [2012] find anthropogenically induced changes in P–E are beginning to emerge for the satellite period using model and reanalysis data. Our analysis focuses on changes in wet and dry regions separately, relying on expected changes from well understood physical processes and the predicted response to warming. It follows the wet and dry regions as they move over time, tracking the changes in these regions independently of their location [Liu et al., 2012] and thus accounting for changes in atmospheric circulation due to natural variability, or in response to warming, for example, poleward migration of the subtropical dry regions [Seager and Naik, 2012].

[5] Climate model simulations of the twentieth century are used to derive fingerprints of precipitation response to all external forcings and greenhouse gas-only forcing. Natural forcing can also affect precipitation. Aerosols from volcanic eruptions reduce precipitation particularly in the wet regions for up to 6 years after the eruption in climate models [Iles et al., 2013]. The eruptions of El Chichon in 1982 and Pinatubo in 1991 may have impacted precipitation during first half of the observation period [Trenberth and Dai, 2007], leading to a naturally forced trends that are similar to those expected due to greenhouse gas forcing.

2. Data: Observations and Models

[6] We use the satellite-based Global Precipitation Climatology Project (GPCP) gridded data set of monthly precipitation [Adler et al., 2003] for the years 1987–2010 (for which measurements from the Special Sensor Microwave Imager are available). Two observational data sets of monthly land precipitation, the Climate Research Unit (CRU) [Harris et al., 2013] and the Global Precipitation Climatology Centre (GPCC) [Schneider et al., 2011] data sets, are included for comparison. The El Niño–Southern Oscillation (ENSO) is

Additional supporting information may be found in the online version of this article.

¹Grant Institute of Earth Science, School of GeoSciences, The University of Edinburgh, Edinburgh, UK.

²University of Reading, Reading, UK.

³National Centre for Atmospheric Science–Climate Division, Walker Institute, University of Reading, Reading, UK.

Corresponding author: D. Polson, School of GeoSciences, Grant Institute, The University of Edinburgh, The King's Buildings, West Mains Road, Edinburgh EH9 3JW, UK. (dpolson@staffmail.ed.ac.uk)

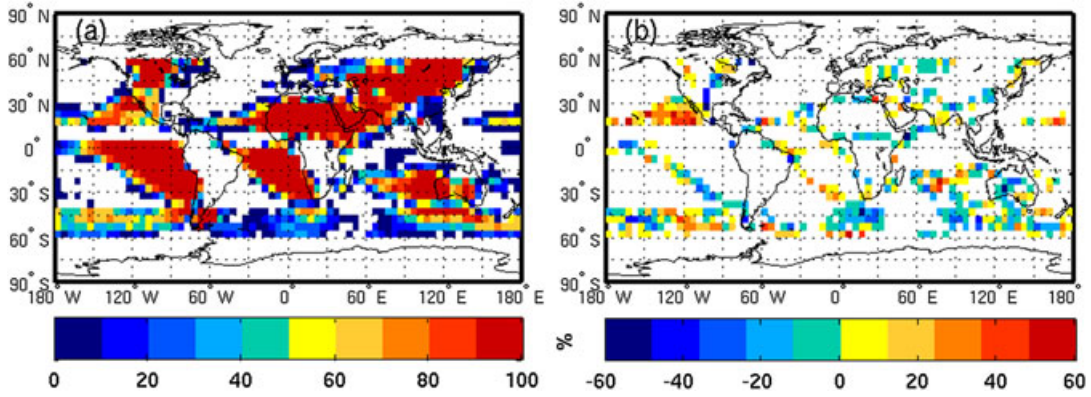


Figure 1. GPCP dry regions for October, November, and December (OND is 1987–2009) from method 1. (a) The percentage of years a gridbox is defined as dry for 1987–2009. (b) Percentage of years dry in 2000–2009 minus 1987–1996, only gridboxes where the change is not zero are plotted. The influence of ENSO is removed from observations. Similar results for other seasons (see supporting information).

removed from the observations as the short record means it will influence the trends (note the supplement discusses the robustness of our findings, including to the removal of ENSO).

[7] Model data are from the Climate Model Intercomparison Project Phase 5 (CMIP5) archive [Taylor *et al.*, 2011]. We use historical runs with anthropogenic and natural forcings (ALL), greenhouse gas-only forcing (GHG), and natural-only forcing (NAT). We also analyze the expected change for 2011–2033, based on the RCP4.5 scenario (Table S1 in the supporting information). Data are aggregated to a $5^\circ \times 5^\circ$ grid and gridboxes split into land and ocean using the model land fraction data with a cutoff of 50%.

3. Analysis of Changes in Wet and Dry Regions

[8] Data were divided into zonal bands from 60°S to 40°S , 40°S to 20°S , 20°S to 0°S , 0°N to 20°N , 20°N to 40°N , and 40°N to 60°N and then split into wet and dry regions (see below). As satellite observations are less reliable poleward of 50° – 55° (G. J. Huffman, personal communication, 2012), the mid- and high-latitudes are excluded from the D+A analysis. The data were grouped into four seasons: January, February, and March (JFM); April, May, and June (AMJ); July, August, and September (JAS); and October, November, and December (OND), to capture the tropical wet and dry seasons, and precipitation averaged across the 3 months. Precipitation changes are calculated for 1988–2010; to ensure OND and JFM are consistent, OND is from the previous year (1987–2009). Two methods are used to define the dry and wet regions in each zonal band, with all D+A analysis using the precipitation changes from Method 1.

[9] *Method 1* uses dry and wet regions of fixed size that move from season to season and year to year. For each zonal band, $\hat{P}_x(i, t)$ is the mean precipitation in the dry or wet region for season i and year t where x is *dry* or *wet*. Gridboxes are sorted from lowest to highest precipitation so that

$$\hat{P}_{\text{dry}}(i, t) = \sum_{n=1}^{L_{33}} P_n(i, t) \quad (1)$$

where P_n is the precipitation in gridbox n and $\hat{P}_{\text{dry}}(i, t)$ is the mean precipitation for all gridboxes in the lower 33.3 percentile ($n \in [1, L_{33}]$), for season i , year t . $\hat{P}_{\text{wet}}(i, t)$ is the mean precipitation of all gridboxes in the upper 33.3 percentile ($n \in [U_{33}, N]$), where N is the total number of gridboxes in each zonal band. A linear least squares regression is used to calculate the change in $\hat{P}_x(i, t)$ over all years, $\dot{P}_x(i)$, where $\dot{P}_x(i)$ is expressed as a percentage relative to $\hat{P}_x(i, t)$ averaged over all years.

[10] *Method 2* uses a fixed cutoff value in each zonal band for dry and wet regions for all years. This allows the regions to move and change size from season to season and year to year. For each zonal band, $P_{33}(i)$ is the 33.3 percentile for all gridboxes, in all years for season i and $P_{66}(i)$ is the 66.67 percentile. If $P_n(i, t)$ are sorted from lowest to highest

$$\hat{P}_{\text{dry}}(i, t) = \sum_{n=1}^{nP_{33}} P_n(i, t) \quad (2)$$

here $n \in [1, n_{P_{33}}]$ are all gridboxes where $P_n(i, t) \leq P_{33}(i)$. For $\hat{P}_{\text{wet}}(i, t)$, $n \in [n_{P_{66}}, N]$ are all gridboxes where $P_n(i, t) \geq P_{66}(i)$. $\dot{P}_x(i)$ is then calculated as in Method 1.

[11] The same methods are applied to individual simulations to calculate $\dot{P}_x(i)$ in each, these are averaged to give the multimodel mean changes. This allows for differences in the precipitation patterns and model error in the location of climatological precipitation. Thus, the model fingerprints are more physically consistent than that obtained by simply averaging across all simulations which may smear out changes.

4. Detection and Attribution

[12] Total least squares regression [Allen and Stott, 2003] determines the magnitude of the fingerprint, \mathbf{F} , of the response to external forcing in the observations \mathbf{y} .

$$\mathbf{y} = (\mathbf{F} + \varepsilon_{\text{finger}}) \cdot \boldsymbol{\beta} + \varepsilon_{\text{noise}} \quad (3)$$

where \mathbf{y} is rank l vector and \mathbf{F} is a $l \times p$ matrix for p external climate forcings. $\boldsymbol{\beta}$ is a vector of scaling factors with p entries giving the magnitude of each fingerprint in the observations, $\varepsilon_{\text{noise}}$ is the residual associated with internal climate

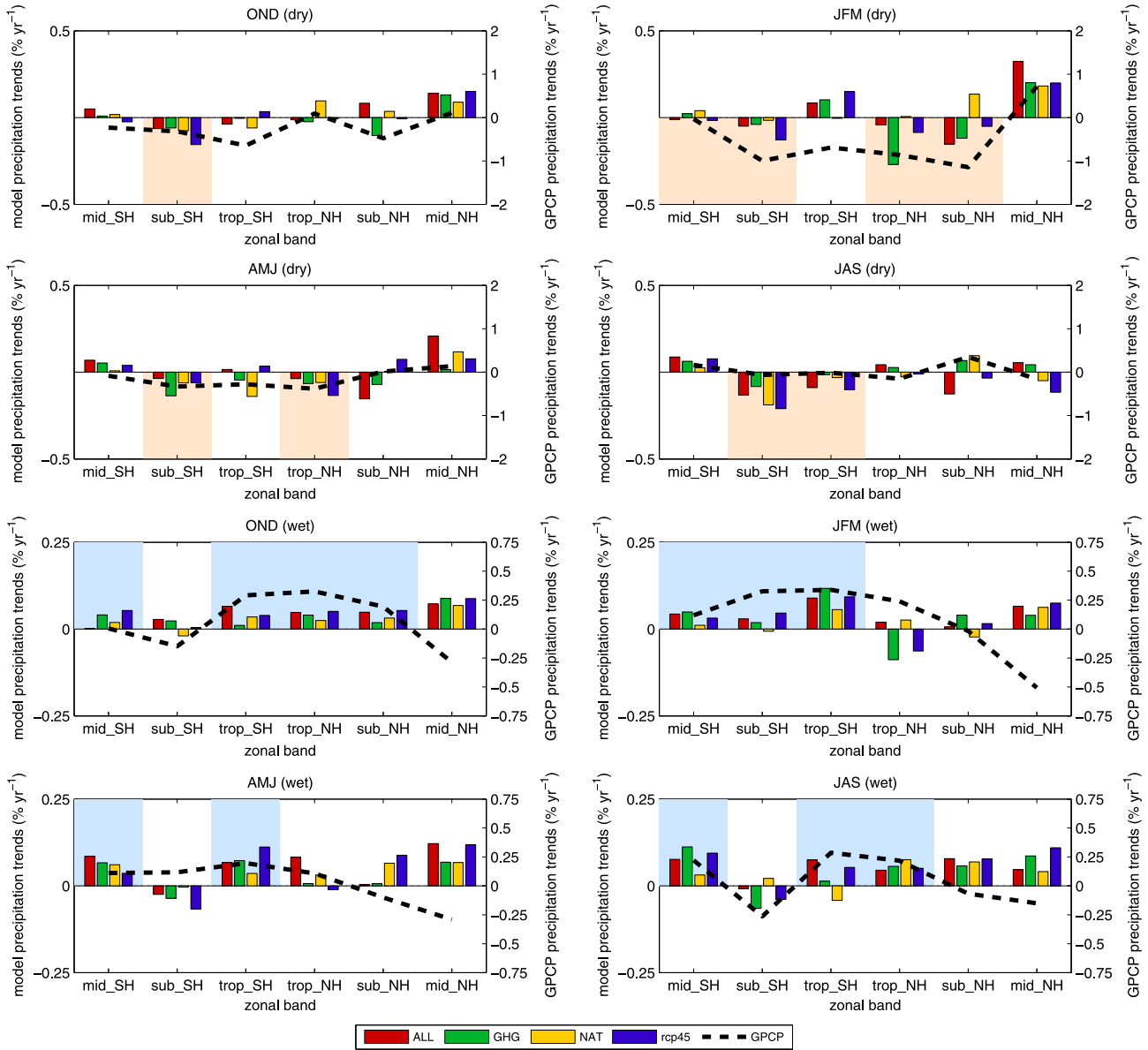


Figure 2. Observed and model-simulated zonal mean changes (% per year) in the dry (top four panels) and wet (lower four panels) regions for land and ocean 1988 to 2010 (OND is 1987–2009). Mid is midlatitudes, sub is subtropical and trop is tropical zonal bands in the Southern Hemisphere (SH) and Northern Hemisphere (NH). The colored bars give the multimodel mean changes for the ALL, GHG, NAT, and RCP4.5 simulations. The orange/blue shading shows where GPCP, ALL, and RCP4.5 are all negative/positive. Note GPCP is plotted on a larger scale, and the influence of ENSO is removed from observations.

variability and is compared to samples of model variability using the f -test [Allen and Stott, 2003]. $\varepsilon_{\text{finger}}$ is a $l \times p$ matrix of variability superimposed on the fingerprint.

[13] Here, single fingerprints ($p = 1$) are used for ALL, GHG, NAT, and RCP4.5. In each case, \mathbf{F} is the multimodel mean $\dot{P}_x(i)$ for the four zonal bands in the tropics and subtropics for seasons $i = 1, 4$, giving $l = 16$ for the dry and wet regions separately and $l = 32$ for the dry and wet regions combined. A two-signal approach was applied to GHG and NAT forcing. All analysis was repeated for land+ocean, land only, and ocean only. Optimized fingerprints were tried but did not improve the signal-to-noise ratio.

[14] Multiple samples of climate noise are added to \mathbf{F} and \mathbf{y} and β recalculated. If $\beta > 0$ at the 5% significance level,

then the fingerprint response pattern is detected in the observations [Hegerl et al., 2007]. As models may underestimate precipitation variability, β is also calculated for double the model variance [Zhang et al., 2007; Polson et al., 2013].

5. Results

[15] The location and size of the GPCP dry and wet regions does not change much from year to year (Figure 1) with 70% to 85% of the dry and wet regions remaining fixed from one year to the next. The models tend to locate the dry and wet regions in the same gridboxes as the observations. If the observations define a gridbox as dry (wet) in over 75%

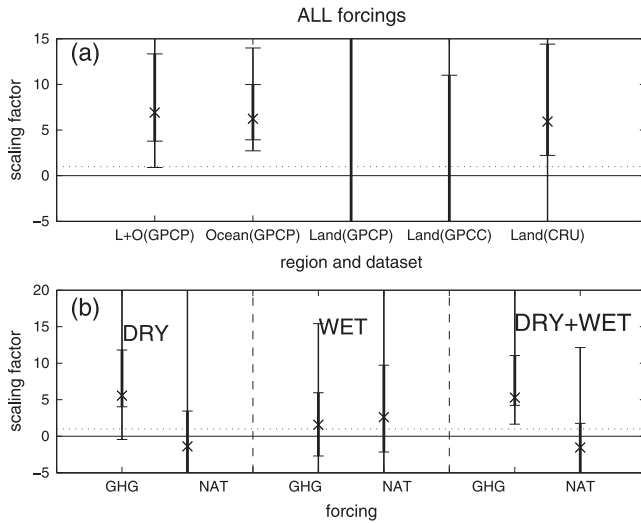


Figure 3. (a) Scaling factors for the wet and dry regions combined using ALL-forced simulations. L+O is land+ocean. (b) Scaling factor for two-signal D+A of GHG and NAT forcing. Crosses show the “best guess” scaling factor for the multimodel mean, thick lines are the 90% confidence interval for the raw model variance added as noise, and thin lines are the 90% confidence interval for double the variance. Influence of ENSO is removed from observations. The residual consistency test is passed in all cases.

of years than on average, 73% (65%) of simulations will also define that gridbox dry (wet) in over 75% of years. The size of the regions from the start to the end of the observation period change by less than the maximum year-to-year variation, except in Southern Hemisphere (SH) midlatitudes.

[16] The tropics and subtropics show a pattern of dry regions becoming drier and wet regions becoming wetter from 1988–2010 for the observations and multimodel means for models with greenhouse gas forcing (ALL, GHG, RCP4.5, see Figure 2). The NAT-only multimodel mean also shows a tendency for dry to get drier and wet to get wetter, but not as consistently for all zonal bands and seasons. However, these patterns are not consistent across all simulations. 20–30% of the ALL, GHG, and RCP4.5, and 40% of the NAT-only individual simulations give more (i.e., zonal bands and seasons) dry regions becoming wetter. Wet regions becoming wetter is a more consistent result with exceptions of less than 10% of the ALL-forced and GHG-only simulations and <20% of the RCP4.5 and NAT-forced simulations. While the pattern of moistening and drying persists over both land and ocean in observations and models (Figures S13 and S14), dry becoming drier is more consistent over oceans than land. Comparison of the GPCP land-only changes with two other station-based observational data sets, GPCC and CRU (masked to the wet and dry regions of GPCP), shows consistency between the data sets (Figures S15 and S16).

[17] The detection analysis for the combined fingerprint of the wet and dry regions and all seasons combined shows that ALL forcing had a significant influence on observed precipitation changes (Figure 3a). The changes from GHG and RCP4.5 simulations are similarly detected in the observed changes, while NAT forcing is not (Figure S17). Changes are also detected over ocean only, but not land only, likely

due to poorer signal-to-noise ratio with a smaller fraction of the wet and dry regions coinciding with land than ocean and a quicker response to more localized forcing [see *Balan Sarojini et al.*, 2012]. SH tropical dry regions in OND and JFM and SH subtropical wet regions in AMJ and JAS were excluded from the land-only analysis because few gridboxes coincide with land.

[18] Changes in the dry and wet regions separately are also detected for ALL, GHG, and RCP4.5 forcing, (over ocean for ALL forcing, Figure S19). The fingerprint of NAT forcing is also detectable for the wet regions, possibly reflecting the influence of volcanoes during the first half of the observation period [*Iles et al.*, 2013]. To distinguish the influence of GHG from NAT forcing, a two-signal D+A was applied, simultaneously estimating GHG and NAT forcing. The results for the combined dry and wet fingerprint show that GHG forcing is detectable while NAT forcing is not (Figure 3b).

[19] Our results were robust to not removing ENSO and using the Niño 3.4 sea surface temperature index from the Climate Prediction Center, NOAA (see supporting information) with two exceptions. When ENSO is not removed, ALL forcing for the dry+wet fingerprint was not detected for land+ocean, while GHG forcing was detectable in the dry regions for the GHG and NAT two-signal analysis.

6. Discussion and Conclusions

[20] Precipitation from GPCP observations and models that include GHG forcing (i.e., ALL, GHG only, and RCP4.5) clearly show a tendency for dry regions to get drier and wet regions to get wetter, consistent with theory [*Allen and Ingram*, 2002; *Held and Soden*, 2006]. The NAT-only simulations show a similar pattern for the wet regions and to a lesser extent in the dry regions due to the influence of the Pinatubo eruption in the first half of the observation period.

[21] The zonal mean changes for the GPCP data are dominated by changes over the ocean which are thought to be less reliable than changes over land [e.g., *Liu et al.*, 2012]. While the pattern of wet regions becoming wetter holds over both land and ocean, drying in the dry regions is less consistent over land. There is evidence that land and ocean precipitation are anticorrelated [*Liu et al.*, 2012]; however, on short timescales, this is due to the influence of ENSO, hence we lose much of this anticorrelation here.

[22] Detection and attribution analysis shows all external forcings and greenhouse forcing are detectable in precipitation changes over the last 20 years in the tropical and subtropical dry and wet regions. Fingerprints based on future change are also detectable showing they are expected to enhance the pattern of change already observed.

[23] If the wet and dry signals are combined, greenhouse gas forcing can be detected separately to natural forcing. The precipitation response to volcanic eruptions in the dry regions is small compared to the greenhouse gas signal, which may explain why the greenhouse gas signal is detectable in the dry regions while the natural signal is not in the one-signal analysis. Our analysis did not include aerosol changes explicitly as not enough runs were available to characterize changes with reasonable signal-to-noise ratio, though aerosols do not change much globally during this period.

[24] Our results are subject to uncertainty in trends derived from satellite data and the shortness of the observational record. However, our results are consistent with results attributing salinity changes to human influences [Durack et al., 2012] over ocean, and changes recorded over land are broadly similar to those recorded by in situ data. Thus, our results suggest an emerging pattern of wet regions becoming wetter and dry regions becoming drier that appears to be at least in part due to greenhouse gas forcing. This provides evidence of an anthropogenically induced intensification of the water cycle.

[25] **Acknowledgments.** We acknowledge the Global Precipitation Climatology Project, the Global Precipitation Climatology Centre, and the Climatic Research Unit. We thank the World Climate Research Programme's Working Group on Coupled Modelling, the climate modeling groups (Table S1), the U.S. Department of Energy's Program for Climate Model Diagnosis and Intercomparison, the Global Organization for Earth System Science Portals. This work was supported by the NERC project PAGODA (NE/I006672/1), the National Science Foundation (ATM-0296007), NCAS, the US Department of Energy's Office of Science, and NOAA's Climate Program Office.

[26] The Editor thanks two anonymous reviewers for their assistance in evaluating this paper.

References

- Adler, R., et al. (2003), The version 2 Global Precipitation Climatology Project (GPCP) monthly precipitation analysis (1979–present), *J. Hydrometeorol.*, *4*, 1147–1167.
- Allen, M., and W. Ingram (2002), Constraints on future changes in climate and the hydrologic cycle, *Nature*, *419*(6903), 224–232.
- Allen, M., and P. Stott (2003), Estimating signal amplitudes in optimal fingerprinting, Part I: Theory, *Clim. Dyn.*, *21*(5), 477–491.
- Balan Sarojini, B., P. A. Stott, E. Black, and D. Polson (2012), Fingerprints of changes in annual and seasonal precipitation from CMIP5 models over land and ocean, *Geophys. Res. Lett.*, *39*, L21706, doi:10.1029/2012GL053373.
- Biasutti, M. (2013), Climate change: Future rise in rain inequality, *Nat. Geosci.*, *6*(5), 337–338.
- Chou, C., J. C. H. Chiang, C.-W. Lan, C.-H. Chung, Y.-C. Liao, and C.-J. Lee (2013), Increase in the range between wet and dry season precipitation, *Nat. Geosci.*, *6*(4), 263–267.
- Durack, P. J., S. E. Wijffels, and R. J. Matear (2012), Ocean salinities reveal strong global water cycle intensification during 1950 to 2000, *Science*, *336*(6080), 455–458.
- Giorgi, F., et al. (2011), Higher hydroclimatic intensity with global warming, *J. Clim.*, *24*(20), 5309–5324.
- Harris, I., P. Jones, T. Osborn, and D. Lister (2013), Updated high-resolution grids of monthly climate observations – the CRU TS3.10 dataset, *Int. J. Climatol.*, doi:10.1002/joc.3711.
- Hegerl, G. C., et al. (2007), Detection of human influence on a new, validated 1500-year temperature reconstruction, *J. Clim.*, *20*(4), 650–666.
- Held, I., and B. Soden (2006), Robust responses of the hydrological cycle to global warming, *J. Clim.*, *19*(21), 5686–5699.
- Iles, C. E., G. C. Hegerl, A. C. Schurer, and X. Zhang (2013), The effect of volcanic eruptions on global precipitation, *J. Geophys. Res. Atmos.*, *118*, doi:10.1002/jgrd.50678.
- Lau, W. K.-M., H.-T. Wu, and K.-M. Kim (2013), A canonical response of precipitation characteristics to global warming from CMIP5 models, *Geophys. Res. Lett.*, *40*, 3163–3169, doi:10.1002/grl.50420.
- Lintner, B. R., et al. (2012), Amplification of wet and dry month occurrence over tropical land regions in response to global warming, *J. Geophys. Res.*, *117*, D11106, doi:10.1029/2012JD017499.
- Liu, C., R. P. Allan, and G. J. Huffman (2012), Co-variation of temperature and precipitation in CMIP5 models and satellite observations, *Geophys. Res. Lett.*, *39*, L13803, doi:10.1029/2012GL052093.
- Liu, C., and R. P. Allan (2013), Observed and simulated precipitation responses in wet and dry regions 1850–2100., *Environ. Res. Lett.*, *8*, 034002, doi:10.1088/1748-9326/8/3/034002.
- Polson, D., G. C. Hegerl, X. Zhang, and T. J. Osborn (2013), Causes of robust seasonal land precipitation changes, *J. Clim.*, *26*, 6679–6697, doi:10.1175/JCLI-D-12-00474.1.
- Santer, B., et al. (2007), Identification of human-induced changes in atmospheric moisture content, *Proc. Nat. Acad. Sci. U.S.A.*, *104*, 15,244–15,253.
- Schneider, U., A. Becker, A. Meyer-Christoffer, M. Ziese, and B. Rudolf (2011), Global precipitation analysis products of the GPCP. <http://gpcc.dwd.de/below> “Publications”.
- Seager, R., and N. Naik (2012), A mechanisms-based approach to detecting recent anthropogenic hydroclimate change, *J. Clim.*, *25*, 236–261.
- Stephens, G. L., and T. D. Ellis (2008), Controls of global-mean precipitation increases in global warming GCM experiments, *J. Clim.*, *21*(23), 6141–6155.
- Sun, Y., S. Solomon, A. Dai, and R. W. Portmann (2007), How often will it rain?, *J. Clim.*, *20*(19), 4801–4818.
- Taylor, K. E., R. J. Stouffer, and G. A. Meehl (2011), An overview of CMIP5 and the experiment design, *Bull. Am. Meteorol. Soc.*, *93*(4), 485–498.
- Trenberth, K. E., A. Dai, R. Rasmussen, and D. Parsons (2003), The changing character of precipitation, *Bull. Am. Meteorol. Soc.*, *84*(9), 1205–1217.
- Trenberth, K. E., and A. Dai (2007), Effects of Mount Pinatubo volcanic eruption on the hydrological cycle as an analog of geoengineering, *Geophys. Res. Lett.*, *34*, L15702, doi:10.1029/2007GL030524.
- Willett, K. M., P. D. Jones, P. W. Thorne, and N. P. Gillett (2010), A comparison of large scale changes in surface humidity over land in observations and CMIP3 GCMs, *Environ. Res. Lett.*, *5*, 025210, doi:10.1088/1748-9326/5/2/025210.
- Zahn, M., and R. P. Allan (2011), Changes in water vapor transports of the ascending branch of the tropical circulation, *J. Geophys. Res.*, *116*, D18111, doi:10.1029/2011JD016206.
- Zhang, X., et al. (2007), Detection of human influence on twentieth-century precipitation trends, *Nature*, *448*(7152), 461–465.